River terrace sand and gravel deposit reserve estimation using three-dimensional electrical resistivity tomography

Chambers, JE[1*], Wilkinson, PB[1], Penn, S[2], Meldrum, PI[1], Kuras, O[1], Loke, MH[3], Gunn, DA[1]

[1]British Geological Survey, Keyworth, Nottingham, NG12 5GG

[2]University of Portsmouth, School of Earth & Environmental Sciences,Portsmouth, PO1 3QL

[3]Geotomo Software Sdn. Bhd., 115, Cangkat Minden Jalan 5, Minden Heights, 11700 Gelugor, Penang, Malaysia

*Corresponding author, email: jecha@bgs.ac.uk, telephone: +44(0)1159363428

ABSTRACT

We describe the application of 3D electrical resistivity tomography (ERT) to the characterisation and reserve estimation of an economic fluvial sand and gravel deposit. Due to the smoothness constraints used to regularise the inversion, it can be difficult to accurately determine the geometry of sharp interfaces. We have therefore considered two approaches to interface detection that we have applied to the 3D ERT results in an attempt to provide an accurate and objective assessment of the bedrock surface elevation. The first is a gradient-based approach, in which the steepest gradient of the vertical resistivity profile is assumed to correspond to the elevation of the mineral/bedrock interface. The second method uses an intrusive sample point to identify the interface resistivity at a location within the model, from which an iso-resistivity surface is identified that is assumed to define the interface. Validation of these methods has been achieved through direct comparison with observed bedrock surface elevations that were measured using real-time-kinematic GPS subsequent to the 3D ERT survey when quarrying exposed the bedrock surface. The gradient-based edge detector severely underestimated the depth to bedrock in this case, whereas the interface resistivity method produced bedrock surface elevations that were in close agreement with the GPS-derived surface. The failure of the gradient-based method is attributed to insufficient model sensitivity in the region of the bedrock surface, whereas the success of the interface resistivity method is a consequence of the homogeneity of the mineral and bedrock, resulting in a consistent interface resistivity. These results highlight the need for some intrusive data for model validation and for edge detection approaches to be chosen on the basis of local geological conditions.

Keywords: electrical resistivity tomography (ERT); aggregates; sand and gravel; mineral exploration; mineral resources; interface detection.

1. INTRODUCTION

Sand and gravel mineral resources are typically evaluated using desk studies, direct investigation using boreholes and trial pits, and material testing to establish particle size distribution and lithology (e.g. Wardrop, 1999; Smith and Collis, 2001). An accurate assessment of the volumes of overburden and mineral, and their distribution across the potential extraction area, is an essential pre-requisite for a mineral reserve assessment and therefore additional information to improve the accuracy and reliability of the geological model can be valuable. Geophysical approaches, including geoelectrical methods, have the potential to improve resource evaluation and reserve estimation by providing information in the gaps between intrusive samples points (Lucius et al., 2006), but have not yet been widely used by the minerals industry for sand and gravel reserve estimation.

Research into the use of 1D resistivity sounding for mineral deposit assessment has produced mixed results (Auton, 1992; Crimes et al., 1994), which led Crimes et al (1994) to conclude that the accuracy of the technique was too poor to be of general use for sand and gravel exploration. One of the earliest references to the application of electrical resistivity tomography (ERT) is by Barker (1997), in which he describes a 2D survey from the Trent Valley, UK. Baines et al. (2002) applied 2D ERT with the aim of assessing its use for investigating aggregate resources, and in particular sand and gravel channel belts and valley fills. They considered sites in the Netherlands, United States and Canada. Beresnev et al. (2002) also sought to develop 2D ERT for sand and gravel prospecting, and used test sites in Iowa, United States to study glacio-fluvial deposits occurring as terraces and point bars. Lucius et al., 2006 considered a range of geophysical methods, including a brief assessment of 2D ERT for deposit evaluation. One of the only examples of the use of 3D ERT for sand and gravel mineral exploration and reserve calculation is given by Chambers et al. (2012), in complex river terrace deposits in the Great Ouse Valley, UK. In addition to work focussed specifically on sand and gravel resource assessment, a number of researchers have considered ERT for the more general, but nevertheless relevant, application of investigating coarse grained unconsolidated Quaternary deposits (e.g. Froese et al., 2005; Kilner et al., 2005; Revil et al., 2005; Turesson et al., 2005)

A significant limitation of ERT using smoothness constrained (Occam) least squares inversion approaches is that the resulting images exhibit smooth gradational variations rather than sharp boundaries, which can make quantification of subsurface structures difficult. Although this can be mitigated by using an L_1-norm (or blocky) inversion, sharp interfaces, such as those between different lithologies, remain indistinct. Consequently, geological boundaries are typically manually inferred from ERT models by visually identifying the steepest resistivity gradient in conjunction with any available ground-truth information (e.g. Sass, 2007). This approach is easily applicable to 2D sections where interfaces can be shown simply as lines, but is more difficult to achieve in 3D models where interfaces are defined by 2D surfaces. More recently, automated methods have been applied for both 2D and 3D datasets (Bouchedda et al., 2012; Chambers et al., 2012; Elwaseif and Slater, 2012; Hsu et al., 2010; Nguyen et al., 2005).

The aim of this work is to assess the potential of 3D ERT for characterising and quantifying mineral reserves. Here we consider economic river terrace sand and gravel mineral deposits overlying clay bedrock. Two methods are considered which automatically extract interface depths from 3D ERT models. The first assumes that the interface is located at the maximum slope of the resistivity-depth curve, and is therefore referred to as the ‘steepest gradient method’ (SGM). The second uses an intrusive sample point to calibrate the model by identifying the resistivity iso-surface associated with the interface, and is referred to here as the ‘known interface method’ (KIM). These approaches have been previously considered by Hsu et al. (2010) and Chambers et al. (2012) for similar applications, using 2D and 3D ERT respectively. In this case, we seek to validate our geophysical results using direct observations of the bedrock surface. This was achieved because, subsequent to the ERT survey, the study site was quarried exposing the bedrock surface. This provided a valuable opportunity for direct comparison of the observed and ERT-derived bedrock surfaces.

2. STUDY SITE

2.1. Location and Background

The site is located at a sand and gravel quarry near Norton Disney, Lincolnshire. The site lies approximately 10 km to the north-east of Newark and the River Trent, and 2 km to the west of the River Witham (Figure 1). At the time of the 3D ERT survey the site was a grassed field bounded by woodland on three sides (north, east and west), with a road on the western edge. The land immediately surrounding the survey area has been worked for sand and gravel for many years. The most recently available borehole data was from 2005, and included holes drilled close to the ERT survey area as shown in Figure 2. Two mineral assessment reports also cover the area immediately around the survey area (Gozzard 1975 and 1976). After the ERT survey had been completed the site was quarried, revealing much of the bedrock across the survey area.

2.2. Geology and hydrogeology

The general geology of the survey area (Berridge et al., 1999) consists of flat lying Lower Lias mudstone bedrock (Jurassic), which is overlain by river terrace deposits of the Balderton Sand and Gravel Member (Quaternary), and a thin layer of topsoil.

The Lias Group is composed predominantly of grey shaly mudstone, with minor limestone, sandstone and ironstone beds. The Norton Disney site is within the lower part of the Lias Group, the Scunthorpe Mudstone Formation. The Scunthorpe Mudstone Formation is characterised by grey, variably calcareous, silty mudstone with numerous thin limestones. The limestones are typically around 0.1-0.3m thick, but can be strong, well cemented and laterally persistent.

The Balderton Sand and Gravel Member is a terrace deposit of the early River Trent, with a surface level at around 14 to 15m above Ordnance Datum (AOD) at the Norton Disney site. Sand and gravel thickness in nearby boreholes is 7.8 to 9.8m. The bulk of the deposit is described from the borehole logs as a brown and yellow-brown slightly silty fine to coarse grained gravelly to very gravelly sand,

and very sandy gravel. A more general description for the Balderton Sand and Gravel (Berridge *et al.*, 1999) describes it as gravel rich, consisting of rounded quartzitic “Bunter” pebbles with subordinate pebble-grade subangular flints and reddish brown Triassic sandstone and siltstone. An overall fining-upward trend is also described, from poorly bedded gravels at the base, to more distinctly bedded, sandier gravels at the top, with a brown to orange-brown sandy, gravelly soil at surface. Particle size analysis indicates 41 to 64% gravel (>4mm), 30 to 55% sand and fine gravel (0.0625mm - 4mm), and 4 to 6% fines (<0.0625mm). Sections in the Balderton Sand and Gravel show cross-bedding and channel infill deposits, both of which were observed in section at the Norton Disney site. Although not observed directly during the site survey, cross bedding and pebble imbrication at other sites further south indicate deposition from river currents flowing towards the north-north-east.

Water levels recorded in lagoons within a few tens of metres of the site indicated that the water level during the survey were likely to have been approximately 4 m below ground level.

3. METHODOLOGY

3.1. Electrical Resistivity Tomography

Resistivity data were collected using an AGI SuperSting R8 eight channel resistivity instrument, multicore cables and stainless steel electrodes. Three-dimensional ERT data collection and modelling methodologies are widely described in the literature (e.g. Wilkinson et al., 2005; Magnusson et al., 2010) and so only a brief summary is presented here.

3.1.1. Survey Design

The 3D ERT survey was carried out within an area of 120 m by 189 m (2.27 hectares); we refer to the long axis of the survey area as *y*, and the short axis as *x*. A summary diagram of the survey grid is shown in Figure 2, with the ERT lines shown in blue. The local origin (x = 0 m, y = 0 m) of the ERT survey area was positioned in the north-western corner of the field. The main survey lines were 189 m long, striking in a north-easterly direction, and were positioned at 6 m intervals to ensure adequate sensitivity to the regions between lines (Gharibi and Bentley, 2005), resulting in a total of twenty one lines. Sixteen additional survey lines, which were 120 m long, were positioned at 12 m intervals perpendicular to the strike of the main survey lines to reduce bias in the data associated with using a single line direction (Chambers et al., 2002). Two additional perpendicular lines were positioned at y = 6 m and y = 186 m to improve image resolution at the north-eastern and south-western margins of the survey. An along-line electrode separation of 3 m was used for all survey lines. The dipole-dipole array with dipole sizes (a) of 3, 6, 9, and 12 m, and dipole separations (na) of $1a$ to $8a$, was used; full sets of reciprocal measurements were collected for each line. The dipole-dipole array was used because it has favourable resolving capabilities relative to other common array types, it can efficiently exploit the multichannel capability of the ERT instrument, and it enables easy collection of reciprocal measurements (Dahlin and Zhou, 2004). The field survey time (i.e. total time on site) was 43 hours; the measurement time (i.e. time taken for ERT instrument to collect the data) was 25 hours.

3.1.2. Data Editing

The combined dataset from the thirty-nine survey lines comprised a total of 46,196 reciprocal pairs. Reciprocal measurements provide the most effective means of assessing data quality and determining reliable and quantitative data editing criteria (e.g. LaBrecque et al., 1996; Wilkinson et al., 2012). Reciprocal error is particularly useful for assessing certain sources of systematic error that are difficult to identify from repeat measurements, e.g. electrode polarisation (Dahlin, 2000). For a normal four-electrode measurement of transfer resistance the reciprocal is found by interchanging the current and potential dipoles. Reciprocal error is defined here as the percentage difference between the normal and reciprocal measurement.

Analysis of the reciprocal errors showed that more than 86 % of the normal and reciprocal measurement pairs had an associated error of less than 5 %. Measurements with a reciprocal error of more than 5 % were removed; the remaining reciprocal pairs were averaged prior to inversion. The mean reciprocal error of the measurements used in the inversion was 0.7% (standard deviation 1%). Contact resistances recorded during the field survey were relatively high, ranging from 2 to 10 kΩ. The consequence of high contact resistances is that less current can be injected into the subsurface, which can reduce signal-to-noise. This probably accounts for the relatively high level of reciprocal errors in excess of 5 %.

3.1.3. Numerical Inversion

Edited survey data collected from the individual lines were concatenated into a single data set comprising 40,079 individual apparent resistivity measurements. The field data were inverted using the regularized least-squares optimization method (Loke and Barker, 1996), in which the forward problem was solved using the finite element method. L1-norm constraints were used on both data and the model, with cutoff factors of 0.05 and 0.01 respectively (Loke and Lane , 2002; Farquharson and Oldenburg, 1998). The L_1-norm (blocky) inversion minimizes the sum of absolute values of the changes in model resistivity and was used in preference to the L_2-norm (smoothness constrained) method, which minimizes the sum of squares, as it provides significantly better results for situations where there are sharp boundaries (Loke et al., 2003). In this case the geology was dominated by the relatively sharp interface between the resistive sand and gravel and more conductive Upper Lias clay.

The resulting resistivity model consisted of 40 cells in the *x*-direction, 63 cells in the *y*-direction and 8 layers in the *z*-direction, resulting in a total of 20,160 model cells. Good convergence between the observed and model data was achieved after 6 iterations, as indicated by an RMS misfit error of 3.2 %. The computational time required was 8.5 hours using a 2.67 GHz Intel i5 Dual-Core system with 8 GB RAM.

3.1.4. Automated interface detection

Here two approaches are considered which automatically extract interface depths from 3D ERT models. The first assumes that the interface is located at the maximum slope of the resistivity-depth curve, and is therefore referred to as the 'steepest gradient method' (SGM). Differential methods of this type are amongst the commonest approaches to interface detection in the field of image analysis (Marr and Hildreth, 1980; Vafidis et al., 2005; Sass, 2007), but automated edge detection has only occasionally been applied to ERT images. The few 2D examples in the literature are provided by Nguyen et al. (2005), Hsu et al. (2010) and Bouchedda et al. (2012). Nguyen et al. (2005) computed gradient images using a maximum directional gradient algorithm from ERT sections generated using the Wenner array and L1-norm inversion; a watershed algorithm was then used to extract crest lines from the gradient images for fault detection. Hsu et al. (2010) successfully applied a Laplacian edge detection method to automatically identify the interface between fluvial deposits and underlying bedrock in ERT sections produced using the pole-pole array and L1-norm inversion. Bouchedda et al. (2012) applied a Canny edge detector with a 2D first derivative operator to identify boundaries in cross-hole ERT images for vadose zone characterisation. Approaches using 3D ERT are described by Chambers et al. (2012) for sand and gravel/bedrock interface detection using the dipole-dipole array and L2-norm inversion and a first derivative edge detector, and Elwaseif and Slater (2012), who used a two-stage inversion approach involving the Robert's edge detector approach on synthetic 3D ERT data sets generated using a dipole-dipole array and L1-norm inversion, which simulated subsurface cavity imaging.

The second approach uses an intrusive sample point, such as a borehole, to calibrate the model by identifying the resistivity iso-surface associated with the interface (e.g. Chambers et al., 2012), and is referred to here as the 'known interface method' (KIM). This is, perhaps, the more intuitive approach, as it relies on interfaces corresponding with resistivity contours, which the eye is naturally drawn to when visually inspecting resistivity sections.

The methods first involved extracting resistivity data, ρ, as a function of depth, z, for each surface position (x, y). An interpolating curve was fitted through $\rho(z)$ for each (x, y) point. In this case, a Piecewise Cubic Hermite Interpolating Polynomial (PCHIP) was that prevents overshoot in the interpolation. The Fritsch-Carlson method (Fritsch and Carlson, 1980) was used to set the coefficients of the polynomial. This method initially uses centred second-order finite-difference estimates of the gradients, which are then modified to ensure that the interpolant is monotonic between data points, is continuous and smooth, and has a continuous (although not necessarily smooth) first derivative. This had the desired effect that the interpolated resistivity preserved the shape of the data and respected its monotonicity. Once the coefficients were determined, the first derivative could be calculated analytically. Then for interface detection using the SGM, the depth corresponding to the steepest gradient on the interpolating curve was identified for each (x, y) point. For the KIM, a known depth to bedrock from a borehole log was used (which in this case was a 'synthetic' borehole – based on a GPS bedrock depth measurement made in the middle of the survey area during excavation). The average model resistivity at this depth in the vicinity of the borehole is denoted ρ_i. The depth to bedrock was then found by calculating where each interpolating curve crosses the line $\rho = \rho_i$. An example set of $\rho(z)$ data and the PCHIP curve from the central region of the ERT survey area is shown in Figure 3.

3.2. Real Time Kinematic global positioning system (RTK-GPS)

Topographic surveys were undertaken before and after the ERT survey using a Leica SmartRover RTK-GPS system. Prior to the ERT survey, the ground surface topography was measured for incorporation in the inversion. During quarrying a topographic survey of the exposed river terrace/bedrock interface was carried out to provide groundtruth data for assessment of the performance of the ERT bedrock detection. Coverage included those areas that were safely accessible on foot, and where the mineral/bedrock interface could be identified. Centimetric resolution was achieved for both position (x, y) and height (z). The mean combined position (x, y) and height (z) co-ordinate quality (Leica Geosystems AG, 2008) of the data recorded during the surveys were 0.057 cm, with a standard deviation of 0.021 cm. Additional uncertainty, of the order of centimetres, was introduced into the measurement, due to the presence of thin patches of gravel and shallow gouging caused by the excavation process.

4. RESULTS AND DISCUSSION

4.1. Three-dimensional resistivity model

The 3D ERT results are given in Figure 4 as a solid model with a series of cut outs, showing the interior of the model. Horizontal and vertical sections through the model are shown in Figure 5.

The river terrace deposits consists of relatively clean sand and gravel, characterized by relatively high resistivities (hundreds of Ωm); the Lower Lias bedrock consists of clay (< 100 Ωm) and is characterized by relatively low resistivities (blue). The good electrical contrast between these two material types permits us to clearly distinguish between them in the 3D resistivity image. The mineral bedrock interface discernible in the model is consistent with that indicated by BH 9/05 (e.g. Figure 4). In this case 3D ERT does not appear to have detected the water level within the sand and gravel.

The high contact resistances observed during the field survey indicate that the topsoil had a relatively low clay content: this is corroborated by the 3D resistivity model. We see that the topsoil resistivities were similar to those of the sands and gravels, and were significantly higher than that of the Lower Lias. However, we do see that topsoil resistivities decreased towards the south-eastern boundary of the model (Figure 4), indicating an increased clay or moisture content in this area. Our analysis of the 3D ERT model suggests that overburden thickness probably increased slightly towards the south-eastern boundary of the site.

Little discernible structure is seen within the main body of the sand and gravel. Figure 5a (x = -4.5 m) shows a depth slice through the terrace deposits; small-scale variations over a distance of a few metres can be observed, but no strong large-scale features indicating significant grainsize variations or channel structures are apparent. A small area centred on x = 100m, y = 100 m shows a slight resistivity high, possibly indicating particularly clean or coarse sand and gravel. A small low resistivity anomaly, parallel to the y-axis can be seen extending from approximately y = 130 m to 189 m; this feature appears to coincide with, and therefore maybe related to, the line of trees and associated root systems extending into the paddock field from the north-eastern site boundary. These results are consistent with visual inspection of working faces during quarrying of the survey area, where clean sand and gravel was observed with little large scale (i.e. metres to tens of metres) variation in clay or fines content.

The interface between the terrace deposits and the Lower Lias does show some variation across the site. Of most significance is the step structure defining a greater depth of sand and gravel on the south eastern boundary of the model; this feature is seen most clearly in the vertical section at y = 94.5 m in Figure 5c, and in the horizontal depth slice at 9 m below ground level in Figure 5b. In this area the interface with the bedrock appears to be ~1 m lower than in much of the rest of the survey area. It is interesting to note that this feature coincides with the low resistivity area at the surface of the model. It is conceivable that these two features are geologically related, e.g. the finer material at the surface may have been deposited in a topographic low caused by the draping of the Balderton Sand and Gravel Member over a bedrock low.

4.2. Determination of Geological Boundaries

The GPS topographic survey of the bedrock surface (Figure 6) covered more than 40% of the original 3D ERT survey area thereby providing a unique comparison dataset with which to assess the ERT results. Complete GPS coverage of the area was prevented by in-situ mineral deposits, access ramps and deep excavations in the quarry floor. The topographic survey confirmed the presence of the step feature (Figure 7a) previously identified from the 3D ERT model (Figure 5). This feature can also be seen in Figure 6, as the water covered area to the east of the excavations.

The results of the SGM and KIM bedrock detections are shown in Figures 7 and 8. The SGM gives an interface (Figure 7b) that is inconsistent with the observed interface depth and morphology (Figure 7a). Compared to the GPS observations of bedrock depth, this method has underestimated the interface depth by a mean value of -3.1m (standard deviation 0.8m). The greatest depths are observed towards the right hand side (south eastern edge) of the survey area, but do not form a consistent step feature.

The average mineral/bedrock interface resistivity value in the region of the synthetic borehole at x = 77 m, y = 100 m was found to be ρ_i = 147 Ωm. The results of the KIM using this value are shown in Figures 7c and 8. Here the bedrock surface is significantly more consistent with the ground truth from the borehole log than the SGM, both in terms of elevation and morphology; the mean difference between the GPS and KIM observations is -0.027m (standard deviation 0.52m). The most significant deviations of the KIM bedrock surface from the GPS observations are concentrated on the edges of the survey area where the model sensitivity, and hence the image resolution, is lowest, and where 3D features adjacent to the survey area can cause artefacts in model. The relative performance of the edge detector at the model boundaries compared to the central regions of the 3D model provides an indication of the likely performance of 2D ERT in this case, which would be similarly influenced by 3D off-line effects.

Comparison of the mean mineral thickness derived from ERT bedrock detection and direct observation (i.e. GPS measurements) indicate that the SGM underestimated these reserves by ~71,000 m^3, or 35% of the total reserves within this area of 205,000 m^3, whilst the KIM is accurate to within ~600 m^3 (or 0.5 % of known reserves).

The failure of the SGM for bedrock detection is in contrast to the positive results achieved using this approach presented by Hsu et al. (2010), and in particular, Chambers et al. (2012) who employed a very similar survey design (i.e. dipole-dipole array, a 3 m along-line electrode separation, and orthogonal line orientations). One of the principal differences between the two studies is the deposit thickness. Chambers et al. (2012) detected an interface with a mean depth below ground level of 3.5 m, compared to 9 m here. The drop in model sensitivity for this resistivity model, which is likely to similar to that of the Chambers et al. (2012) survey, between 3.5 m and 9 m below ground level is approximately an order of magnitude (Figure 3), which indicates that the resolution of the interface in this study will be significantly worse than for the previous study. Due to the low sensitivity of the model at these depths to the measured data, it is probable that the underestimation of the interface depth is because the sharp boundary produced by the L_1-norm inversion has been positioned one or two model blocks above the true location of the bedrock surface.

These limitations of the SGM at depth can be demonstrated by a simple synthetic modelling exercise in which a horizontally stratified sand and gravel deposit (ρ = 900 Ωm) overlying clay bedrock (ρ = 20 Ωm) was simulated for mineral thicknesses ranging from 1 m to 15 m (Figure 9a). The mineral and bedrock resistivities were chosen to reflect those observed during the field survey (e.g. Figure 4). Resistance data were calculated for the surface array configurations used during the field surveys, and inverted using the L_1-norm method. SGM interface depths were calculated from the inverted resistivities along a vertical profile in the centre of the model. A summary plot showing the true and SGM interface depths determined from the inverted models is shown in Figure 9b. Three key points can be drawn from these results. The first is that the accuracy of the SGM depth to bedrock determination generally decreases with increasing depth (or with decreasing image resolution). For bedrock depths within the range considered during the field survey significant inaccuracies (i.e. > 2 m) are apparent. The second is that the influence of the model discretization can be seen (particularly for the deeper interfaces) where the SGM depths are similar for different true depths due to the SGM interface being forced onto model block boundaries. The third is that the SGM tends to underestimate the true depth, which is again consistent with the results of the field survey.

The performance of the KIM described here is significantly better than in the cases given by Hsu et al. (2010) and Chambers et al. (2012). In both these previous studies the near surface fluvial deposits displayed a significantly greater degree of heterogeneity, with a great range of resistivities at the mineral/bedrock interface, which prevented a single resistivity value satisfactorily defining the interface. In this study, both the Balderton Sand and Gravel Member and the Lias Clay bedrock are relatively homogeneous in terms of resistivity, which has resulted in the successful application of the KIM.

5. Conclusions

In this study 3D ERT has revealed the structure of an economic fluvial sand and gravel deposit, including a relatively subtle (i.e. approximately ~1 m relief) erosional structure on the clay bedrock surface beneath ~9 m of mineral. Two bedrock detection algorithms were applied to the 3D ERT model and were validated against direct observations of the bedrock surface, which was partially revealed during quarrying. The gradient based edge detector (SGM) failed in this case because it incorrectly placed the sharp boundary between model blocks at a higher level in the model – this is attributed to very low model sensitivity in the region of the interface. Conversely, the KIM, which relies on at least one intrusive sample point to guide bedrock surface identification, was successful.

Comparison of these results with those of other studies clearly shows that geological conditions (in terms of depth to bedrock and heterogeneity) are a critical consideration when determining appropriate bedrock detection approaches. Although, the SGM has been successfully applied elsewhere in similar studies, the influence of model sensitivity in the region of the interface is a limiting factor, which highlights the need for corroboration of model results with intrusive sample points. Improvement in the performance of the SGM could therefore probably be achieved by using optimised survey design, which has been demonstrated to improve model resolution for deeper regions of the subsurface when compared to standard array types (Loke et al., 2010; Wilkinson et al., 2006 and 2012). In this case, the relative homogeneity of the deposit resulted in the successful application of the KIM, whereas it is unlikely to be a viable approach for highly variable deposits.

6. Acknowledgements

The research was funded by Defra through the MIST Programme (Grant MA/7/G/1/007), and in-kind contributions from project partners. The authors wish to thank the project partners, and CEMEX in particular, for their contributions to the project. This paper is published with the permission of the Executive Director of the British Geological Survey (NERC).

7. References

Auton, C. A., 1992. The Utility of Conductivity Surveying and Resistivity Sounding in Evaluating Sand and Gravel Deposits and Mapping Drift Sequences in Northeast Scotland. Engineering Geology. 32, 11-28.

Baines, D., Smith, D. G., Froese, D. G., Bauman, P., Nimeck, G., 2002. Electrical resistivity ground imaging (ERGI): a new tool for mapping the lithology and geometry of channel-belts and valley- fills. Sedimentology. 49, 441-449.

Barker, R. D., 1997. Electrical imaging and its application in engineering investigations. In: D. M. McCann, M. Eddleston, P. J. Fenning, G. M. Reeves, Eds.), Modern Geophysics in Engineering Geology. The Geological Society, London, pp. 37-44.

Beresnev, I. A., Hruby, C. E., Davis, C. A., 2002. The use of multi-electrode resistivity imaging in gravel prospecting. Journal of Applied Geophysics. 49, 245-254.

Berridge, N G, Pattison, J, Samuel, M D A, Brandon, A, Howard, A S, Pharaoh, T C, & Riley, N J. 1999. Geology of the Grantham district. *Memoir of the British Geological Survey*, Sheet 127 (England and Wales).

Bouchedda, A., Chouteau, M., Binley, A., Giroux, B., 2012. 2-D joint structural inversion of cross-hole electrical resistance and ground penetrating radar data. Journal of Applied Geophysics, 78, 52-67.

Chambers, J.E.; Wilkinson, P.B.; Wardrop, D.; Hameed, A.; Hill, I.; Jeffrey, C.; Loke, M.H.; Meldrum, P.I.; Kuras, O.; Cave, M.; Gunn, D.A.. 2012 Bedrock detection beneath river terrace deposits using three-dimensional electrical resistivity tomography. Geomorphology. 10.1016/j.geomorph.2012.03.034 (In Press)

Chambers, J E, Ogilvy, R D, Kuras, O, Cripps, J C, And Meldrum, P I, 2002. 3D electrical imaging of known targets at a controlled environmental test site. *Environmental Geology*, Vol. 41, 690-704.

Crimes, T. P., Chester, D. K., Hunt, N. C., Lucas, G. R., Mussett, A. E., Thomas, G. S. P., Thompson, A., 1994. Techniques Used in Aggregate Resource Analyses of 4 Areas in the Uk. Quarterly Journal of Engineering Geology. 27, 165-192.

Dahlin, T, 2000. Short note on electrode charge-up effects in DC resistivity data acquisition using multi-electrode arrays. Geophysical Prospecting. Vol. 48 (1), 181-187.

Dahlin, T., Zhou, B., 2004. A numerical comparison of 2D resistivity imaging with 10 electrode arrays. Geophysical Prospecting. 52, 379-398.

Elwaseif, M and Slater, L, 2012. Improved Resistivity Imaging of Targets with Sharp Boundaries Using an Iterative Disconnect Procedure. Journal of Environmental and Engineering Geophysics, 17 (2), 89-101.

Farquharson, C.G., Oldenburg, D.W., 1998. Nonlinear inversion using general measures of data misfit and model structure, Geophysical Journal International, 134 (1), 213-227.

Fritsch, F.N., Carlson, R.E., 1980. Monotone piecewise cubic interpolation. SIAM Journal on Numerical Analysis. 17, 238–246.

Froese, D. G., Smith, D. G., Clement, D. T., 2005. Characterizing large river history with shallow geophysics: Middle Yukon River, Yukon Territory and Alaska. Geomorphology. 67, 391-406.

Gharibi, M., Bentley, L. R., 2005. Resolution of 3-D electrical resistivity images from inversions of 2-D orthogonal lines. Journal of Environmental and Engineering Geophysics. 10, 339-349.

Gozzard, J R, 1975. The sand and gravel resources of the country around Besthorpe, Nottinghamshire. Description of 1:25 000 resource sheet SK 86 and part of SK 76. Mineral Assessment Report 17, HMSO.

Gozzard, J R, 1976. The sand and gravel resources of the country east of Newark upon Trent, Nottinghamshire. Description of 1:25 000 resource sheet SK 85. Mineral Assessment Report 20, HMSO.

Hsu, H. L., Yanites, B. J., Chen, C. C., Chen, Y. G., 2010. Bedrock detection using 2D electrical resistivity imaging along the Peikang River, central Taiwan. Geomorphology. 114**,** 406-414.

Kilner, M., West, L. J., Murray, T., 2005. Characterisation of glacial sediments using geophysical methods for groundwater source protection. Journal Of Applied Geophysics. 57, 293.

Labrecque, D. J., Miletto, M., Daily, W., Ramirez, A., Owen, E., 1996. The effects of noise on occam's inversion of resistivity tomography data. Geophysics. 61, 538-548.

Leica Geosystems AG, 2008. Leica GPS1200+ Technical Reference Manual. 733512-7.0.0en.

Loke, M. H., Lane, J. W., 2002. The use of constraints in 2D and 3D resistivity modelling. 8th meeting of the European Section of the Environmental and Engineering Society, Aveiro, Portugal, pp. 4.

Loke, M. H., Acworth, R. I., Dahlin, T., 2003. A comparison of smooth and blocky inversion methods in 2D electrical imaging surveys. Exploration Geophysics. 34, 182-187.

Loke, M. H., Barker, R. D., 1996. Practical techniques for 3D resistivity surveys and data inversion. Geophysical Prospecting. 44, 499-523.

Loke, M.H., Wilkinson, P.B., and Chambers, J.E., 2010. Fast computation of optimized electrode arrays for 2D resistivity surveys. Computers and Geosciences, 36, 1414-1426.

Lucius, J E, Langer, W H, And Ellefsen, K J, 2006. An Introduction to Using Surface Geophysics to Characterize Sand and Gravel Deposits. U.S. Geological Survey, Open-File Report 2006-1257, Magnusson, M. K., Fernlund, J. M. R., Dahlin, T., 2010. Geoelectrical imaging in the interpretation of geological conditions affecting quarry operations. Bulletin of Engineering Geology and the Environment. 69, 465-486.

Marr, D. and Hildreth, E., 1980. Theory of edge-detection. Proceedings of the Royal Society of London Series B-Biological Sciences 207, 187-217.

Nguyen, F., Garambois, S., Jongmans, D., Pirard, E., Loke, M.H., 2005. Image processing of 2D resistivity data for imaging faults. Journal of Applied Geophysics, 57(4), 260-277.

Revil, A., Cary, L., Fan, Q., Finizola, A., Trolard, F., 2005. Self-potential signals associated with preferential ground water flow pathways in a buried paleo-channel. Geophysical Research Letters. 32, L07401.

Sass, O., 2007. Bedrock detection and talus thickness assessment in the European Alps using geophysical methods. Journal of Applied Geophysics, 62(3), 254-269.

Smith, M R, and Collis, L, 2001. Aggregates: Sand, gravel and crushed rock aggregates for construction purpose. Geological Society Engineering Geology Special Publications, The Geological Society.

Turesson, A., Lind, G., 2005. Evaluation of electrical methods, seismic refraction and ground-penetrating radar to identify clays below sands - Two case studies in SW Sweden. Near Surface Geophysics. 3, 59.

Vafidis, A., Economou, N., Ganiatsos, Y., Manakou, M., Poulioudis, G., Sourlas, G., Vrontaki, E., Sarris, A., Guy, M., and Kalpaxis, T., 2005. Integrated geophysical studies at ancient Itanos (Greece). Journal of Archaeological Science 32, 1023-1036.

Wardrop, D. R., 1999. A study on the accuracy of sand and gravel reserve estimates. Quarterly Journal of Engineering Geology. 32, 81-86.

Wilkinson, P. B., Chambers, J. E., Meldrum, P. I., Ogilvy, R. D., 2005. A comparison of self-potential tomography with electrical resistivity tomography for the detection of abandoned mineshafts. Journal of Environmental and Engineering Geophysics. 10, 381-389.

Wilkinson, P., Loke, MH, Meldrum, PI, Chambers, JE, Kuras, O, Gunn, DA, and Ogilvy, RD., 2012. Practical aspects of applied optimised survey design for Electrical Resistivity Tomography. Geophysical Journal International. 189, 428-440.

Wilkinson, P B, Chambers, J E, Meldrum, P I, and Ogilvy R D, 2006. Optimization of array configurations and geometries for the detection of abandoned mineshafts by 3D cross-hole electrical resistivity tomography. Journal of Environmental and Engineering Geophysics, 11, 213 - 221.

List of Figures

Figure 1. Geological map of the Newark area, including the study site. Inset map (top left) shows the location of the study area at the national scale.

Figure 2. Annotated aerial photograph of the survey area, showing the 3D ERT survey grid and borehole locations.

Figure 3. Resistivity data (circles) and interpolating curve (black line) as a function of elevation (and depth), at x = 77 m, y = 100 m. The points of steepest gradient and where the curve crosses the interface resistivity value are indicated. Model sensitivity data (grey circles) and interpolating curve (grey line) are shown for the same vertical profile.

Figure 4. 3D resistivity model showing sands and gravels of the Balderton Member (yellow-red) overlying Lias Group mudstone bedrock (blue). Approximate interface location between the mineral and bedrock shown as a dashed white line.

Figure 5. Horizontal sections through the 3D ERT model at (a) z = -4.5 m and (b) -9 m below ground level, and a vertical section at (c) y = 94.5 m. The location of the vertical section (c) is indicated by a black line of the horizontal sections (a and b).

Figure 6. Photograph of survey area during the ERT survey (left) and during quarrying (right), showing the northern (N) and eastern (E) corners of the survey area (arrows), the geological interface between the sand and gravel and the Lias Clay (solid line), and the approximate location of the step feature on the bedrock surface defining a topographic low to the south (dashed line).

Figure 7. Lias clay bedrock surface recovered using (a) real-time-kinematic GPS measurements of the excavated surface, (b) the known interface method (KIM), and (c) the steepest gradient method (SGM). Difference plots of (d) GPS-SGM and (e) GPS-KIM. GPS measurement locations shown as black dots.

Figure 8. Distributions of elevation differences between real-time-kinematic GPS and the SGM (grey) and KIM (black) derived bedrock surfaces respectively.

Figure 9. (a) Synthetic model of sand and gravel overlying clay bedrock from which dipole-dipole array (*a* = 3, 6, 9 and 12 m, *n* = 1-8) measured resistances were calculated for models comprising mineral thicknesses ranging from 1 to 15 m, and (b) the results of SGM analysis of inverted model results.

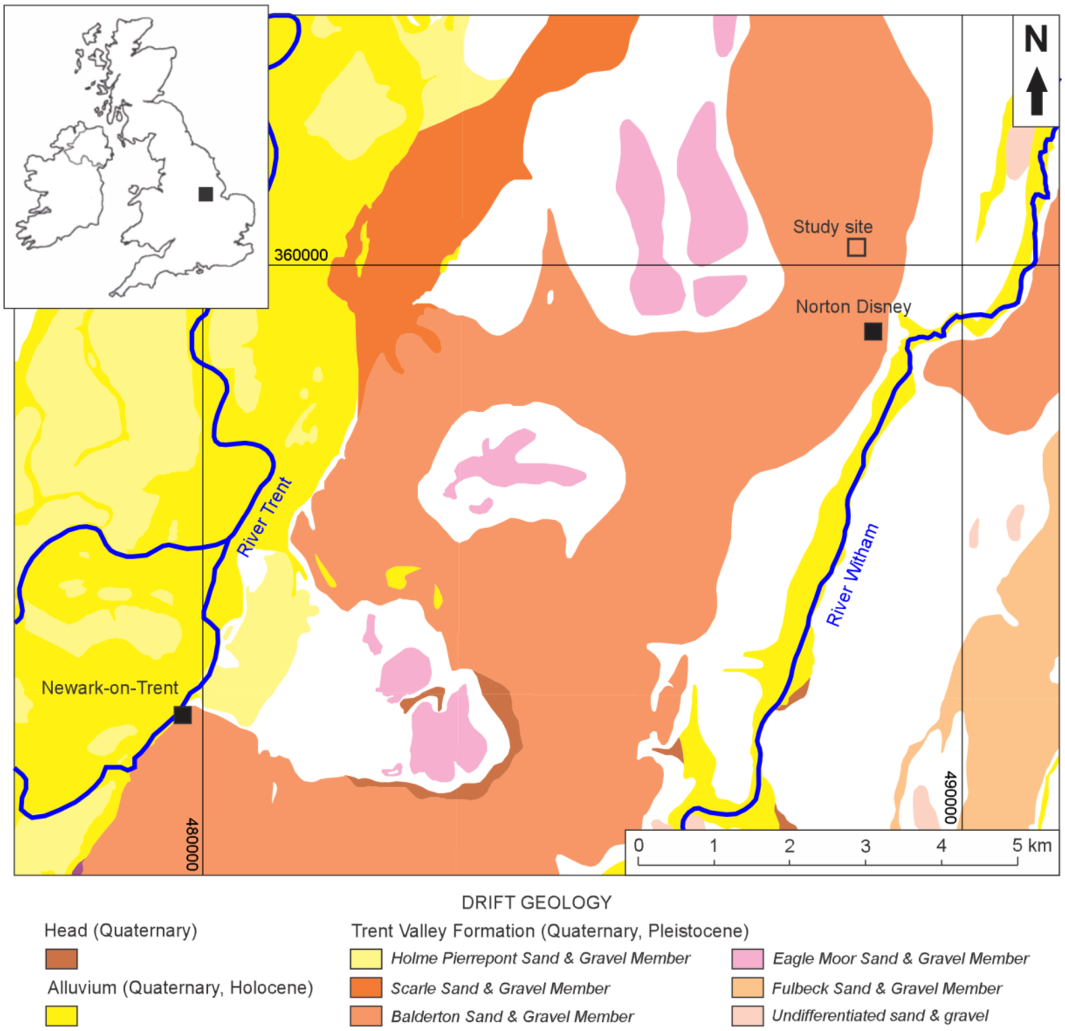

Figure 1. Geological map of the Newark area, including the study site. Inset map (top left) shows the location of the study area at the national scale.

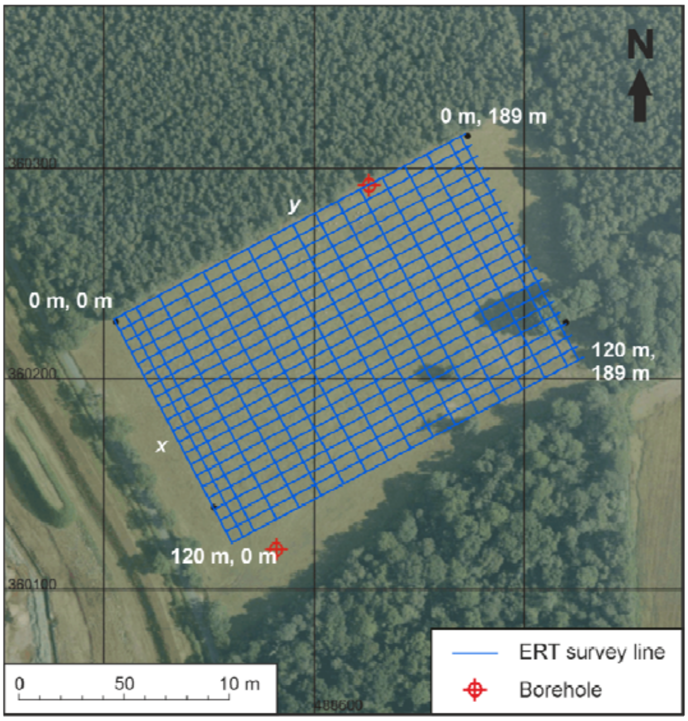

Figure 2. Annotated aerial photograph of the survey area, showing the 3D ERT survey grid and borehole locations.

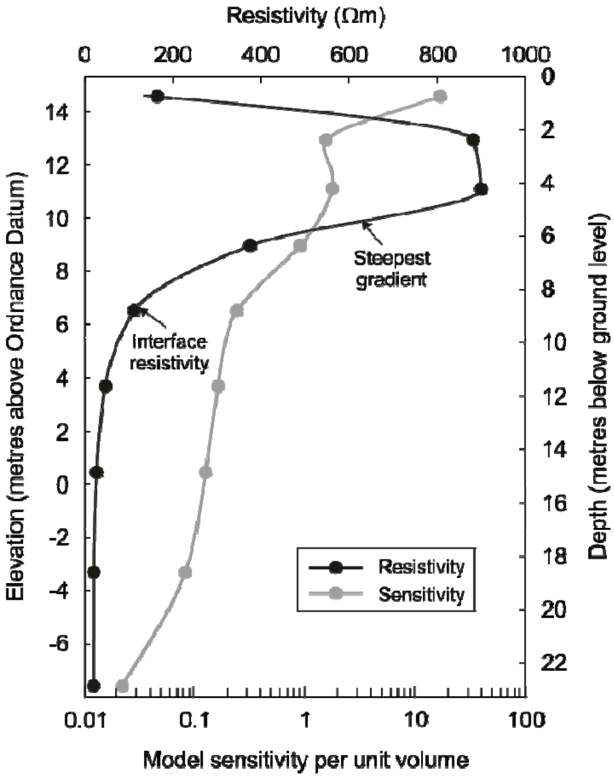

Figure 3. Resistivity data (circles) and interpolating curve (black line) as a function of elevation (and depth), at x = 77 m, y = 100 m. The points of steepest gradient and where the curve crosses the interface resistivity value are indicated. Model sensitivity data (grey circles) and interpolating curve (grey line) are shown for the same vertical profile.

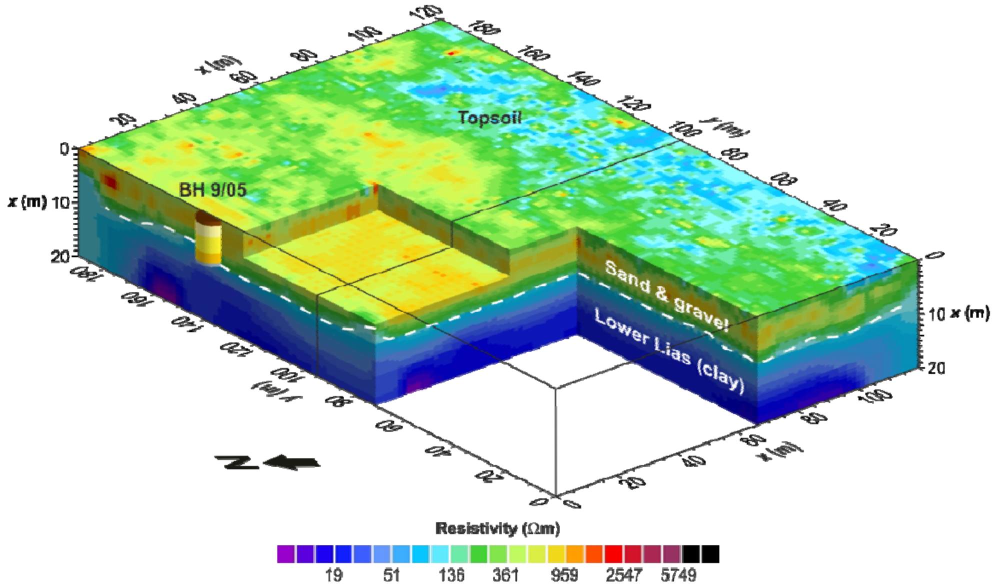

Figure 4. 3D resistivity model showing sands and gravels of the Balderton Member (yellow-red) overlying Lias Group mudstone bedrock (blue). Approximate interface location between the mineral and bedrock shown as a dashed white line.

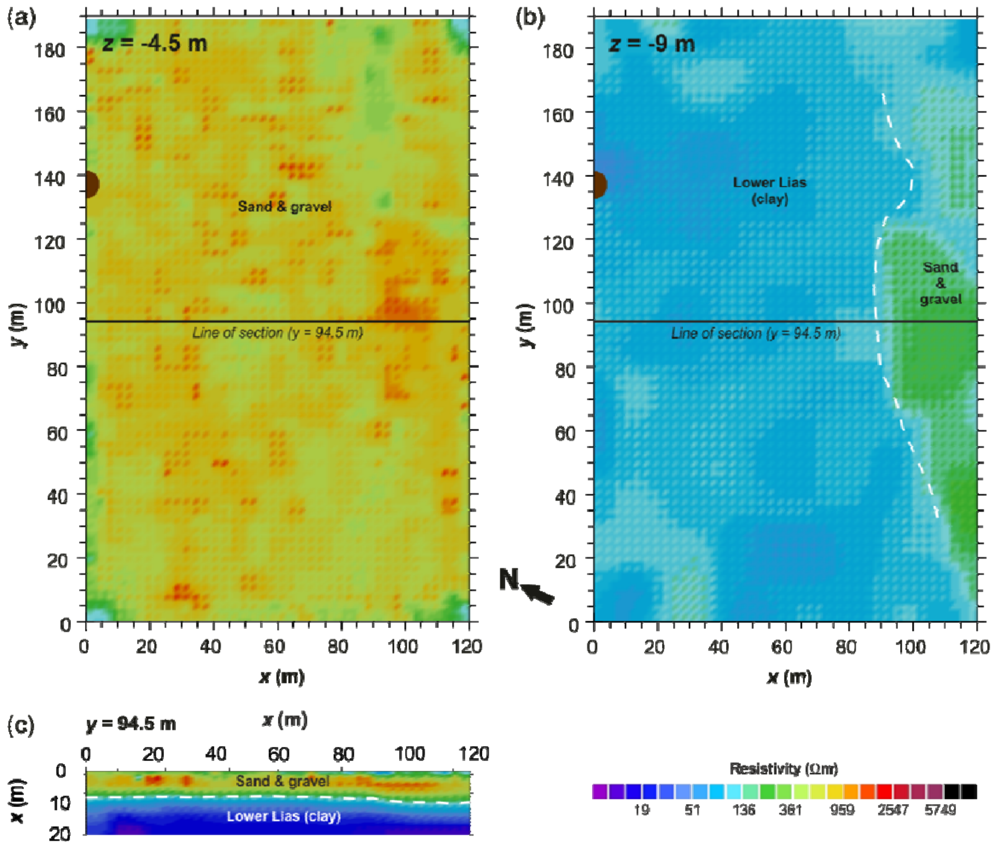

Figure 5. Horizontal sections through the 3D ERT model at (a) z = -4.5 m and (b) -9 m below ground level, and a vertical section at (c) y = 94.5 m. The location of the vertical section (c) is indicated by a black line of the horizontal sections (a and b).

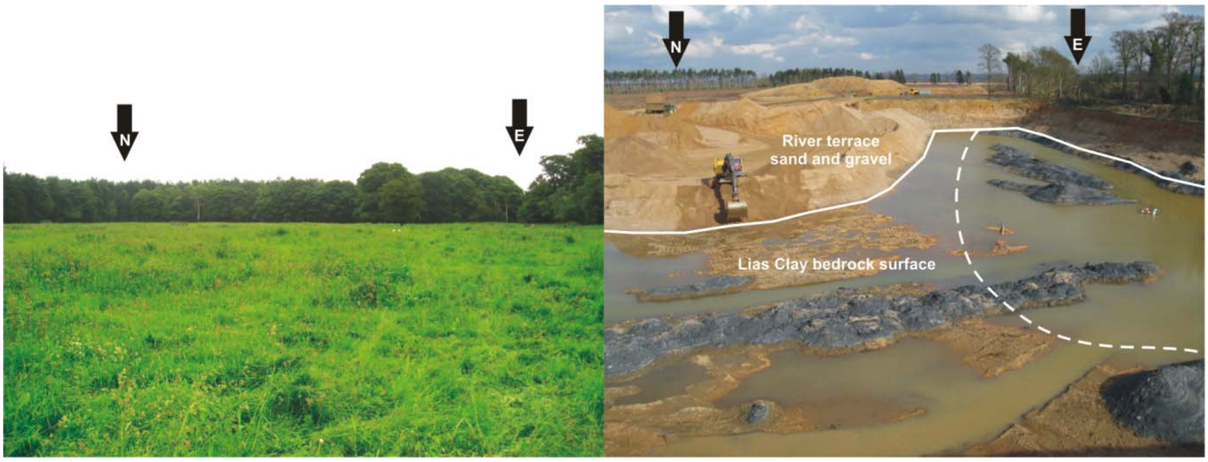

Figure 6. Photograph of survey area during the ERT survey (left) and during quarrying (right), showing the northern (N) and eastern (E) corners of the survey area (arrows), the geological interface between the sand and gravel and the Lias Clay (solid line), and the approximate location of the step feature on the bedrock surface defining a topographic low to the south (dashed line).

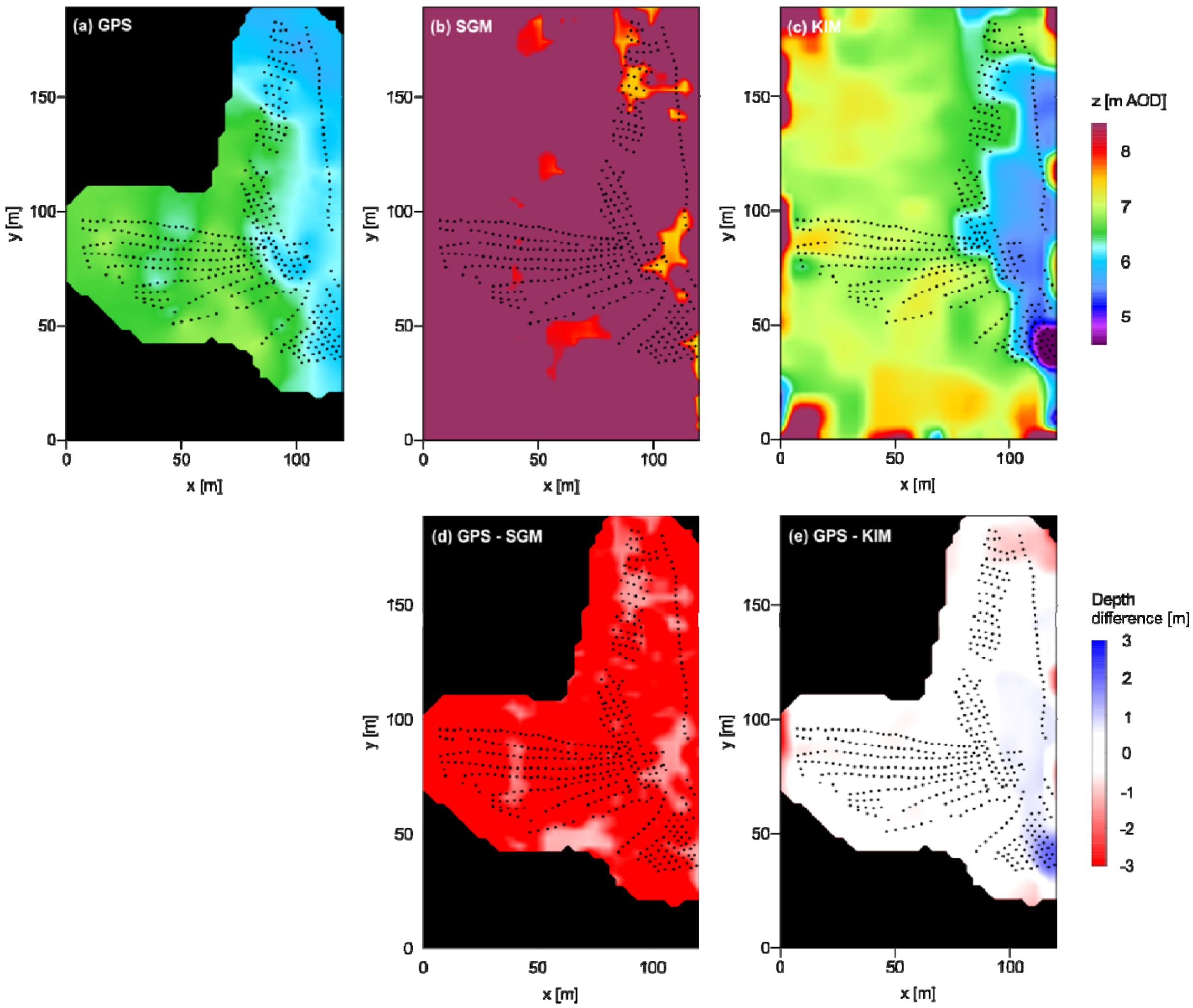

Figure 7. Lias clay bedrock surface recovered using (a) real-time-kinematic GPS measurements of the excavated surface, (b) the known interface method (KIM), and (c) the steepest gradient method (SGM). Difference plots of (d) GPS-SGM and (e) GPS-KIM. GPS measurement locations shown as black dots.

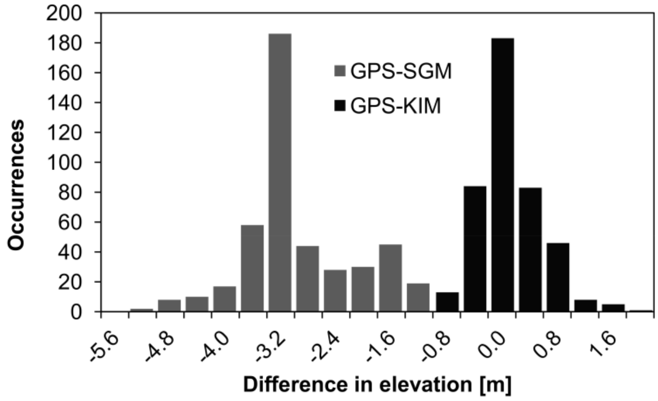

Figure 8. Distributions of elevation differences between real-time-kinematic GPS and the SGM (grey) and KIM (black) derived bedrock surfaces respectively.

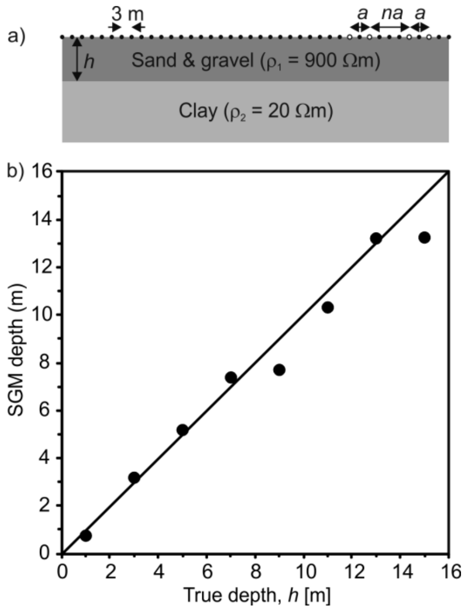

Figure 9. (a) Synthetic model of sand and gravel overlying clay bedrock from which dipole-dipole array (*a* = 3, 6, 9 and 12 m, *n* = 1-8) measured resistances were calculated for models comprising mineral thicknesses ranging from 1 to 15 m, and (b) the results of SGM analysis of inverted model results.